Journal of Theoretical and Applied Mechanics, Sofia, 2012, vol. 42, No. 2, pp. 3–42

SOLID MECHANICS

FRACTURE IN COMPOSITES – AN OVERVIEW (PART I)*

V. I. Rizov
Department of Technical Mechanics,,
University of Architecture, Civil Engineering and Geodesy,
1, Chr. Smyrnensky Blvd, 1046 Sofia, Bulgaria,
e-mail: V_RIZOV_FHE@UACG.BG

[Received 12 April 2012. Accepted 14 May 2012]

Abstract. An overview of the literature for the last twenty years on the fracture mechanics of unidirectional fibre reinforced polymer composites is presented. Pure mode (I, II, and III) as well as mixed mode longitudinal cracks (i.e., cracks that prolongate along the fibres) are considered mainly. It is shown that the strain energy released rate is the most widely used parameter for fracture toughness characterization. Various solutions for determination of the strain energy release rate in composites using linear-elastic fracture mechanics are presented. Studies on fracture in composite sandwich structures are reviewed, too. Some analyses of damages and their influence on fracture behaviour also are considered. Topical problems of composite fracture mechanics are formulated.
Key words: Crack, fibre reinforced composite, beam, fracture mechanics.

1. Introduction

Recently, the application of fibre reinforced composite materials in various branches of the techniques (mechanical engineering, shipbuilding, aeronautics, civil engineering, car industry) has undergone a huge development. The basic advantage of the composites is their high strength-to-weight ratio in comparison with the conventional structural materials. Therefore, they are very suitable for application in load-bearing structures, where the low weight is of primary concern. In the civil engineering, the composites are used for

*The financial support of project BG051PO001–3.3.05.–0001 "Science and business", funded on Operational program "Development of human resources" at the "European social fund" is highly appreciated.

reinforcing of concrete structures [1, 2, 3, 4, 5, 6, 7, 8, 9]. Studies on application of composites for strengthening of steel bridges have been published, too [10, 11, 12]. Technologies have already been developed for reinforcing masonry walls by composites [13, 14, 15].

In the present article, unidirectional fibre reinforced composites are considered mainly. Their increasing application is due to well developed manufacturing technologies [16, 17, 18, 19, 20, 21]. Unidirectional fibre reinforced composites possess high strength and stiffness in the fibre direction. However, their tensile strength in transverse direction (i.e., perpendicular to the fibres) is relatively low. Therefore, they are rather susceptible to initiation and growth of longitudinal cracks (i.e., cracks which propagate along the fibres). Usually, the cracking is related to the presence of various internal defects (voids, flows, imperfections, fibre debonds, microcracks, and cavities), mostly formed during the composite manufacturing [22, 23, 24, 25, 26, 27, 28, 29, 30, 31]. Similar damages may also arise during lifetime of the structure due to thermomechanical loads, fatigue or impact events. The defects and damages act as stress concentrators, from which crack initiation and propagation takes place in he fibre direction. The cracks may reduce significantly the strength and stiffness of the composite. Thus, the load-bearing capacity of a structure is highly dependent on the fracture toughness properties of the composite. The poor resistance to cracking is one of the major limitation factors for constructive applications of the composites. Therefore, the analysis of cracks in composites is an important problem of the fracture mechanics.

In the present paper, an overview is reported on the characteristic fracture studies for the last twenty years. Topical problems of fracture mechanics of composite materials are formulated.

2. Three basic approaches in fracture mechanics

2.1. Stress intensity factors

Cracks in composites are analyzed using the methods of fracture mechanics. The origin of fracture mechanics can be found in the fundamental work of Griffith [32], who analyzed the strength of glass considering the stability of a small crack.

An important step in the development of fracture mechanics is the stress analysis in the vicinity of the uniaxially loaded crack (Fig. 1) performed by Westergaard [33]. He found that the stresses at a point P can be expressed

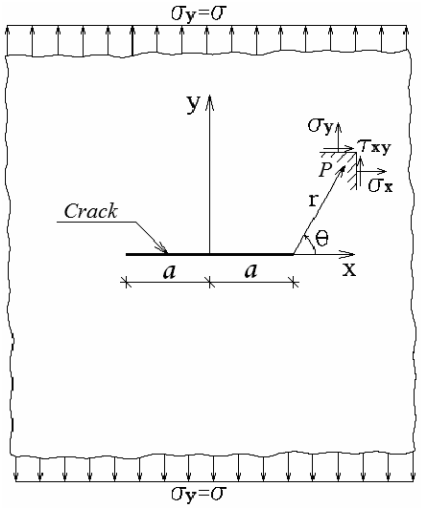

Fig. 1. Stress components at the crack tip area

as:

$$\sigma_x = \frac{K_I}{\sqrt{2\pi r}} f_1(\theta), \tag{1}$$

$$\sigma_y = \frac{K_I}{\sqrt{2\pi r}} f_2(\theta), \tag{2}$$

$$\tau_{xy} = \frac{K_I}{\sqrt{2\pi r}} f_3(\theta), \tag{3}$$

where r and θ are polar coordinates, K_I is the stress intensity factor for the crack opening mode, $f_i(\theta)$ are trigonometric functions of the angle θ.

The three pure modes of fracture are depicted in Fig. 2. One may observe that the difference between them is in the pattern of crack deformation: opening of crack (mode I), in-plane shear of crack (mode II), and anti-plane shear of crack (mode III). Each pure mode of fracture is characterized by the corresponding stress intensity factor. For instance, since the crack in Fig. 1 is subjected to opening, the mode I stress intensity factor, K_I, participates in the formulae for the stresses (1), (2), and (3). We have the stress intensity factor K_{II} in the same way for the in-plane shear mode and for the anti-plane shear mode the stress intensity factor is K_{III}. It should be noted that the expressions for stress distributions for cracks under pure mode II and pure mode III

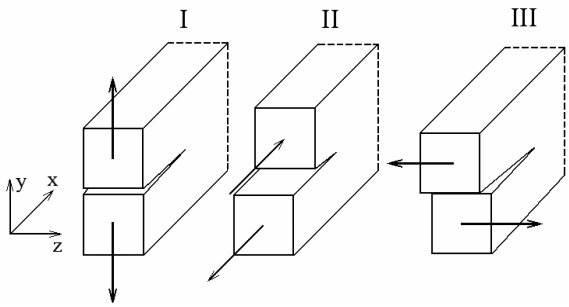

Fig. 2. The three pure modes of crack deformation.

loading conditions are similar to Eqs. (1), (2), and (3). The most important parameter in these expressions is the stress intensity factor. Therefore, obtaining of solutions for the stress intensity factors for certain loading conditions and crack geometries is one of the basic problems of fracture mechanics [34]. Analyses of stress intensity factors can be found in Refs. [35, 36, 37, 38, 39, 40]. The stress intensity factors may be used to predict the onset of crack growth. For this purpose, the following criterion is applied:

$$K_I = K_{IC}, \tag{4}$$

where K_I is the mode I stress intensity factor for the investigated crack geometry, K_{IC} is the critical value of the stress intensity factor. K_{IC} is known as fracture toughness. It is a material property which can be determined experimentally. The criteria for crack growth onset for other modes of crack loading are similar to Eq. (4). The major disadvantage of the stress intensity factor approach is that a crack tip stress field analysis is required.

2.2. Strain energy release rate

A more useful approach is the strain energy release rate. The strain energy release rate, G, for a body of constant thickness, b, is defined by:

$$G = \frac{F^2}{2b}\frac{dC}{da}, \tag{5}$$

where F is the load, $a$is the crack length. The system compliance is given by:

$$C = \frac{\delta}{F}, \tag{6}$$

where δ is the displacement at the point of load application. It is obvious, that one may determine G by plotting C as a function of a and finding the curve

slope, $\frac{dC}{da}$, corresponding to the load value F. Thus, the basic advantage of Eq. (5) is that crack tip stress field analysis is not needed. The function $C = C(a)$ may be obtained from measurements on a fracture test specimen. Another way for obtaining the function $C = C(a)$ is to find an analytical solution that relates the load F, to the corresponding displacement, δ (it should be noted that for interlaminar fracture test specimens such solutions usually may be found).

It should also be mentioned that the strain energy release rate is related to the stress intensity factors K_I, K_{II},and K_{III}. The relationship for a mode I crack under plane strain is:

$$G_I = \frac{K_I^2\left(1-\nu^2\right)}{E}, \tag{7}$$

where E and ν are the modulus of elasticity and the Poisson's ratio, respectively. The relationship for a mode II crack is similar to Eq. (7), i.e.:

$$G_{II} = \frac{K_{II}^2\left(1-\nu^2\right)}{E}. \tag{8}$$

In a case of mode III crack G_{III} is related to K_{III} by:

$$G_{III} = \frac{K_{III}^2\left(1+\nu\right)}{E}. \tag{9}$$

It is clear that if the strain energy release rate mode components are determined from experiments, Eqs. (7), (8), and (9) may be applied to calculate the stress intensity factors (this is very useful in the cases when the crack tip stress field analysis is rather complicated).

The crack growth onset criterion for pure mode I loading conditions in the terms of strain energy release rate possess the form:

$$G_I = G_{IC}, \tag{10}$$

where G_I is the strain energy release rate calculated for the considered crack configuration, G_{IC} is the critical value of the strain energy release rate (G_{IC} is a material parameter which can be determined from mode I fracture tests). The crack growth onset criteria for other modes of fracture are similar to Eq. (10).

The total value of strain energy release rate for a crack under mixed-mode loading conditions may be obtained by the method of superposition. Thus, for a crack under general mixed-mode I/II/III loading we have:

$$G = G_I + G_{II} + G_{III}, \tag{11}$$

where G_I, G_{II}, and G_{III} are the mode I, mode II, and mode III components of the strain energy release rate, respectively.

2.3. *J*-integral

The J-integral is another frequently used approach for analysis of cracks.

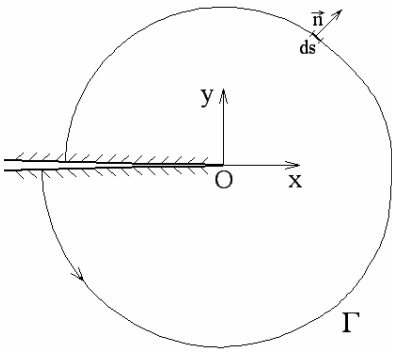

Fig. 3. Integration path around the crack

This is a path-independent contour integral introduced by Rice [41]. It is shown, that the J-integral uniquely characterizes the fracture behaviour of non-linear materials [42, 43]. The J-integral is given by

$$J = \int_{\Gamma} \left(w dy - T_i \frac{\partial u_i}{\partial x} ds \right), \tag{12}$$

where Γ is an arbitrary counter-clockwise path around the crack tip (Fig. 3), w is the strain energy density, T_i are the traction vector components, u_i are the components of the displacement vector, and ds is a length increment along the path Γ. It should be specified that the traction vector defines the normal stresses acting at the contour. J is called a path-independent integral, because its value is independent of the integration path around the crack. The J-integral can be used for both linear-elastic and non-linear elastic materials. The J-integral value is equal to the strain energy release rate for the case of linear-elastic behaviour. Thus, J for a mixed-mode I/II/III crack under plane strain may be determined using the relationship:

$$J = G = G_I + G_{II} + G_{III} = \frac{1-\nu^2}{E}\left(K_I^2 + K_{II}^2\right) + \frac{1+\nu}{E} K_{III}^2. \tag{13}$$

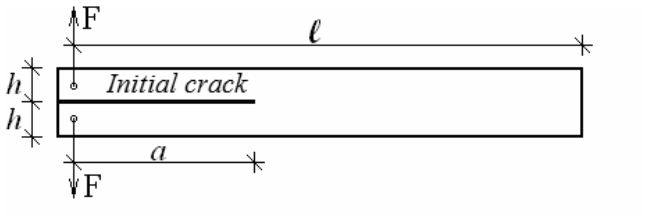

Fig. 4. Double cantilever beam specimen

An important advantage of the J-integral approach is that it may also be applied for analysis of cracks in elastic-plastic materials, provided no unloading occurs.

The crack growth onset criterion for mode I fracture using the J-integral is expressed as:

$$J_I = J_{IC}, \tag{14}$$

where J_{IC} is a material property which can be determined from experiments. Criteria for other modes of fracture are similar to Eq. (14).

3. Fracture studies

It is a common practice to characterize the fracture behaviour of composite materials, using beam specimens. They contain an initial crack and are loaded properly in order to generate the desired mode of fracture. The test methods use pure and mixed-mode interlaminar fracture beam specimens. Therefore, fracture analysis of composite beams is an important issue not only from theoretical, bur also from practical view point.

Mode I interlaminar fracture has received considerable attention in specialized literature [44, 45, 46, 47, 48, 49, 50, 51, 52, 53, 54, 55, 56, 57, 58, 59, 60, 61, 62].

The most frequently used test method for experimental investigation of such fracture is the Double Cantilever Beam (DCB) shown in Fig. 4. The cross-section of the beam is a rectangular. In its middle plane the DCB specimen possesses an initial crack of length a. The specimen is loaded transversely as illustrated in Fig. 4, so that pure mode I crack opening deformation occurs. The basic purpose of the testing is to determine the critical load value F_C, which corresponds to the crack growth onset. F_C is needed to calculate the critical value of the mode I strain energy release rate (i.e., the mode I fracture toughness) G_{IC}, which is used in the criterion (10). The following formula has

been obtained applying linear-elastic fracture mechanics for the strain energy release rate in the DCB [58]:

$$G_{IC} = \frac{12F_C^2 a^2}{b^2 h^3 E_1}, \tag{15}$$

where b and h are the width and the height of the specimen cross-section, respectively. E_1 is the longitudinal modulus of elasticity. The experimental data indicate that the relationship between the load and its application point is linear up to the crack growth onset [46]. Thus, linear-elastic fracture mechanics (which is based on the assumption for validity of the Hook's law) may be applied for analysis of G_{IC} in the DCB specimen. The experimental data show also that the crack propagates straight along the initial crack direction, i.e. the crack path is a straight line. This is due to the fact that the crack propagates in the matrix parallel to the reinforcing fibres.

An experimental and analytical investigation on the influence of the low temperature on the mode I interlaminar fracture behaviour of glass-epoxy laminates was conducted using the DCB test [63]. The fracture toughness was characterized in terms of the critical strain energy release rate using the compliance method. It was found that G_{IC} can be related to the experimentally measured specimen compliance C, by the formula:

$$G_{IC} = \frac{3}{2H}\left(\frac{F_C}{B}\right)^2 \frac{(BC)^{2/3}}{\alpha_1}, \tag{16}$$

where F_C is the critical load (at which the crack growth initiation is observed), α_1 is a parameter fitted to the test data, B and H are the width and the height of the specimen cross-section, respectively.

The influence of low temperatures on mode I intrerlaminar fracture behaviour was investigated also by Humer et al. [64]. The interface between fibre reinforced plastics and copper in the crack opening mode of deformation was studied, too.

Mode I intrerlaminar fracture toughness of glass fibre reinforced composites with fibre surface treatment was studied using DCB specimens in Ref. [46]. A linear-elastic beam theory analysis was performed in order to calculate the strain energy release rate. The test data were analyzed also by the compliance method using Eq. (5). The effect of geometrical variations on the fracture behaviour was evaluated, too.

A beam model based on adhesion theory was developed to study the DCB specimen in Ref. [65]. A closed form solution was obtained to predict the

external loads leading to intrerlaminar fracture. The results were compared with data available in the literature. It was found, that the model is very useful for parametric analyses of the interlaminar fracture behaviour of laminated beam structures.

The interlaminar fracture behaviour of continuous carbon fibre/epoxy composites under pure mode I crack loading is investigated using DCB test specimens in Ref. [66]. A beam theory analysis based on linear-elastic fracture mechanics was carried-out to calculate the mode I strain energy release rate.

Linear-elastic beam theory model was developed for analytical evaluation of the fracture toughness (defined as the critical strain energy release rate) from test data in Ref. [67]. Fracture testing was performed at a constant displacement rate. A graph of the load versus the displacement response was generated. The measured critical load value at the onset of the crack growth was used to obtain the fracture toughness by the compliance method. For this purpose, the specimen compliance was measured at various crack lengths. It was found that the compliance was related to the crack length by a power function:

$$C = Ra^n, \tag{17}$$

where R and n are parameters which were determined using the method of least squires. Eq. (17) was differentiated with respect to the crack length. The result was substituted in Eq. (5), i.e.:

$$G_{IC} = \frac{F_C^2 nRa^{n-1}}{2b}, \tag{18}$$

where F_C is the measured critical load value at the onset of crack growth.

Fracture toughness of carbon fibre reinforced composites was characterized in terms of critical strain energy release rate using the DCB test method in Ref. [68]. The experimentally obtained load-crack opening displacement diagrams were linear up to the point at which the crack growth initiation occurred. Liner-elastic fracture mechanics was applied to analyze the interlaminar fracture behaviour. Strain energy release rate was calculated from the test data using a beam theory model involving the crack opening displacement at the point of load application.

The relative displacements in the pure mode II crack deformation of the two arms are directed longitudinally, i.e. parallel to the crack direction (Fig. 2).

Loading conditions for generating such mode of fracture can be achieved in the End Notch Flexure (ENF) beam specimen shown in Fig. 5 [69, 70, 71,

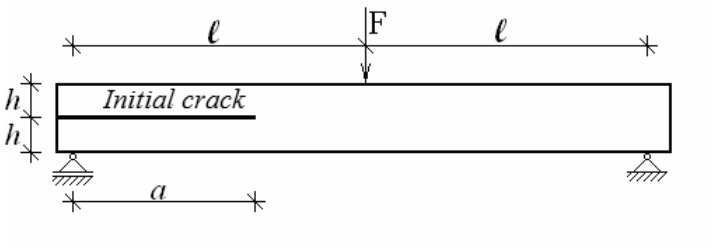

Fig. 5. End notch flexure specimen

72, 73, 74, 75, 76, 77, 78, 79, 80]. An initial interlaminar crack of length a is introduced in the beam middle plane. The beam is loaded in three point bending. It is obvious that the stress state of the two crack arms is antisymmetric with respect to the crack plane. The experiments show that when the load reaches its critical value F_C, the crack propagates straight along the direction of initial crack [81]. The test data indicate also that the load-displacement diagram is linear up to the crack growth initiation. During the experiments it is observed that there are no residual (i.e., permanent) displacements in the ENF specimens, since the load-displacement diagram 'returns' to the origin of the coordinate system after unloading. These experimental findings are a clear indication for the applicability of linear-elastic fracture mechanics. The critical strain energy release rate for the ENF specimen is expressed as [46]:

$$G_{IIC} = \frac{9F_C a^2 \delta}{2b\,(3a^2 + 2l^3)}, \tag{19}$$

where F_C is the critical load (at which the crack growth begins), α is the crack length, δ is the displacement of the application point of load, b is the width of the beam cross-section. l is one half of the beam span. Eq. (19) is obtained using linear-elastic beam theory.

Mode II interlaminar fracture behaviour of glass-cloth/epoxy laminates was studied in Ref. [81]. The effects of low temperature and geometrical variations were thoroughly analyzed. ENF tests were conducted using stroke control mode with a constant crosshead speed of 0.5 mm/min. Load-displacement curves were plotted for each tests. All specimens were split open after testing in order to examine the fracture surfaces by scanning electron microscopy. The mode II intrerlaminar fracture toughness was characterized in terms of the critical strain energy release rate using a beam theory model. The experimentally measured critical load values and the specimen compliance were needed for the application of the model.

The influence of fibre volume fraction on the mode II interlaminar fracture toughness of glass/epoxy composite was investigated by Davies et al. [82]. Mode II fracture tests were carried-out on ENF beam specimens with fibre volume fraction from 42% to 65%. The critical strain energy release rate was calculated by the compliance method. For this purpose, the following compliance expression was used:

$$C = C_0 + ma, \tag{20}$$

where C is the specimen compliance, a is the interlaminar crack length. The mode II critical strain energy release rate was obtained applying Eq. (5) as:

$$G_{IIC} = \frac{F_C^2 m}{2b}, \tag{21}$$

where F_C is the critical load, b is the specimen width, $m$is the slope of the compliance versus crack length plot. The analysis revealed that the fracture toughness decreases quite substantially with increasing fibre content. This finding was attributed to the thick resin rich layer in the low fibre content composites.

The ENF test method was applied to study the interlaminar fracture behaviour of carbon/polyetheretherketone composites in Ref [83]. Special attention was paid to the influence of specimen geometry on the mode II fracture toughness. For this purpose, ENF specimens with various span-length-to-specimen-thickness ratios were tested. All tests were performed with a crack-length-to-span-length ratio of 0,5. The load-displacement curves were linear up to the crack growth initiation point for all tested specimens. Thus, a linear-elastic beam theory model was applied to evaluate the mode II critical strain energy release rate from the test data. It was found that the interlaminar fracture behaviour was independent of specimen geometry, provided that the span-length-to-specimen-thickness is greater than 20 and that a film separator is inserted between the crack surfaces.

The mode II fracture toughness of carbon fibre composites was investigated via the ENF test also by Bullions et al. [68]. A support span to thickness ratio of 0.2 was used. The load was applied during testing to the specimens using a constant crosshead speed of 5.3 mm/min. All specimens exhibited linear-elastic behaviour confirming the applicability of Eq. (19) for calculation of G_{IIC}.

The ENF specimens were used to obtain the mode II critical strain energy release rate of unidirectional glass fibre reinforced composite with fibre

surface treatments [46]. The loading during the test was realized through a displacement rate of 1.0 mm/min. The critical load and the corresponding displacement were measured at the beginning of the crack growth. A conventional linear-elastic beam analysis was performed to calculate the G_{IIC}.

Interlaminar fracture behaviour of alumina fibre reinforced epoxy laminates under mode II loading was investigated using the ENF beam specimen [84]. Both 3-point and 4-point ENF tests were conducted. The experimentally obtained specimen compliance was expressed as a function of crack length. The strain energy release rate was calculated by the compliance method.

The composite structures in the engineering practice very often are subjected to combined loadings which create conditions for initiation and growth of mixed-mode I/II interlaminar cracks. Therefore, it is important to develop methods for theoretical analysis and experimental characterization of mixed-mode I/II interlaminar fracture behaviour.

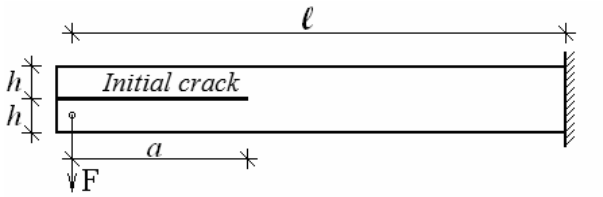

Fig. 6. Asymmetrical double cantilever beam specimen

For this purpose, several specimen configurations and test procedures were proposed. Among them very popular is the Asymmetric Double Cantilever Beam (ADCB) specimen illustrated in Fig. 6 [85, 86, 87, 88, 89, 90, 91, 91, 92]. An initial crack of length a is introduced in the beam middle plane. The lower crack arm is loaded by a concentrated force F. The critical value of the total strain energy release rate can be calculated by the formula:

$$G_{I/IIC} = \frac{21F_C^2a^2}{4b^2E_1h^3}, \tag{22}$$

where F_C is the critical load value at the onset of crack growth, E_1 is the longitudinal modulus of elasticity, b is the width of the beam cross-section. Eq. (22) is obtained using the conventional linear-elastic beam theory. It is found also, that the mixed-mode ratio G_I/G_{II}, is equal to 1,333 and is independent of the applied load and the crack length. The test data available in the literature indicates that linear-elastic fracture mechanics can be applied for analysis of the ADCB specimens [92].

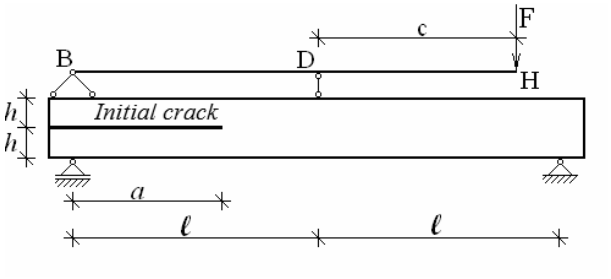

Fig. 7. Mixed mode bend specimen

Another widely used configuration for experimental investigation of mixed-mode I/II interlaminar fracture behaviour is the Mixed-Mode Bend (MMB) specimen presented in Fig. 7 [93, 94, 95, 96, 97, 98, 99, 100, 101, 102].

The specimen has an initial interlaminar crack of length a located at the mid-thickness. A downward load is applied on the lever arm. Thus, the upper end block (at the cracked end of the specimen) is pulled upwards and a downward load is applied to the specimen centre. In this way, mixed-mode I/II crack loading conditions are generated. A linear-elastic beam theory analysis of the MMB specimen yielded the following expression for the critical value of the total strain energy release rate [103, 104]:

$$G_{I/IIC} = \frac{3a^2F_C^2}{16b^2h^3l^2E_1}\left[4\left(3c-l\right)^2+3\left(c+l\right)^2\right], \tag{23}$$

where b is the width of the specimen cross-section. The analysis revealed also that the mixed-mode ratio G_I/G_{II}, depends on the lever arm length c. The mixed-mode ratio can be varied also by changing the position of the loading roller D (Fig. 7). Thus, the MMB specimen facilitates experimental characterization of mixed-mode I/II interlaminar fracture toughness over a wide range of mixed-mode ratios.

Mixed-mode I/II interlaminar fracture experiments were conducted on unidirectional glass/epoxy laminates using MMB specimens in Ref. [102]. The strain energy release rate was calculated by Eq. (5). The experimental compliance law was expressed as:

$$C = \alpha + \beta a^3, \tag{24}$$

where the material parameters α and β were determined by interpolating the measured load point compliances for different mixed-mode I/II ratios.

MMB test method was applied to study the mixed-mode I/II interlaminar fracture behaviour of a carbon/epoxy composite by Asp et al. [105]. A linear-elastic beam theory analysis was carried-out to calculate the strain energy release rate based on the obtained results from the experiments.

Influence of elevated temperature on fracture behaviour of a carbon/epoxy composite was studied in Ref. [106]. The MMB test was employed for investigation of mixed-mode I/II cracking. The interlaminar fracture toughness referred to the strain energy release rate is obtained at the crack growth initiation. The MMB specimen was analyzed by a model based on linear-elastic fracture mechanics.

Strain energy release rate can be calculated by the virtual crack closure technique for more complicated crack problems. This is a widely used approach which assumes validity of linear-elastic fracture mechanics [107, 108, 109]. Its application is based on results obtained by means of finite element analysis. The strain energy release rate components associated with the three basic modes of crack growth can be computed separately by this technique.

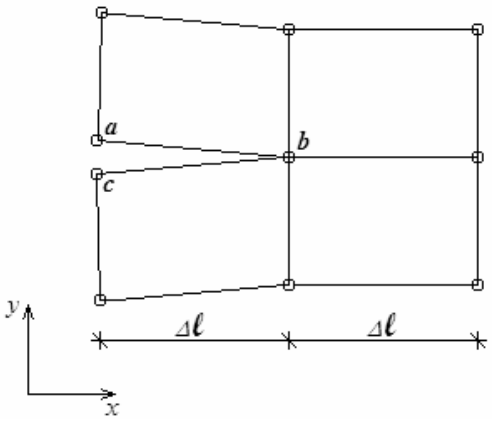

Fig. 8. Mesh scheme with four-nodded elements in crack tip area

The basic advantage of this technique is that it requires only one analysis by the finite element model for the actual crack length. The nodal forces at the crack tip and the nodal displacement behind the crack tip determined by the finite element analysis are needed to compute the strain energy release rate mode components. A two-dimensional finite element mesh in the crack tip area is presented schematically in Fig. 8. Four-nodded elements are used. The virtual crack closure technique assumes that the work performed to closure

the crack by one element is equal to the strain energy released when the crack grows by one element length. Therefore, at node b in Fig. 8 the strain energy release rate mode components can be expressed as:

$$G_I = \frac{1}{2\Delta l}\left[Y_b\left(v_a - v_c\right)\right], \tag{25}$$

$$G_{II} = \frac{1}{2\Delta l}\left[X_b\left(u_a - u_c\right)\right], \tag{26}$$

where X and Y are the nodal force components, and u and v are the nodal displacement components in the x and y directions, respectively. The subscripts in Eqs (25) and (26) denote the corresponding nodes in Fig. 8.

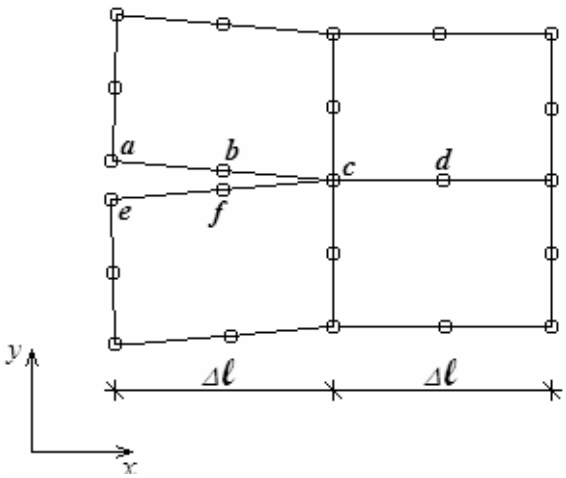

Fig. 9. Mesh scheme with eight-nodded elements in crack tip area

The strain energy release rate mode components if the mesh is developed using eight-nodded elements (Fig. 9) are approximated by:

$$G_I = \frac{1}{2\Delta l}\left[Y_c\left(v_a - v_e\right) + Y_d\left(v_b - v_f\right)\right], \tag{27}$$

$$G_{II} = \frac{1}{2\Delta l}\left[X_c\left(u_a - u_e\right) + X_d\left(u_b - u_f\right)\right]. \tag{28}$$

Let us now consider a 3-D problem. Schematic of crack front area is depicted in Fig. 10. Eight-nodded spatial elements are used. The strain energy release rate mode components at node i can be expressed as:

$$G_I = \frac{1}{2\Delta a \Delta b}\left[Z_i\left(w_r - w_s\right)\right], \tag{29}$$

$$G_{II} = \frac{1}{2\Delta a \Delta b}\left[X_i\left(u_r - u_s\right)\right], \tag{30}$$

$$G_{III} = \frac{1}{2\Delta a \Delta b}\left[Y_i\left(v_r - v_s\right)\right], \tag{31}$$

where X, Y, and Z are nodal force components, and u, v, and w are nodal displacement components in the x, y, and z directions, respectively.

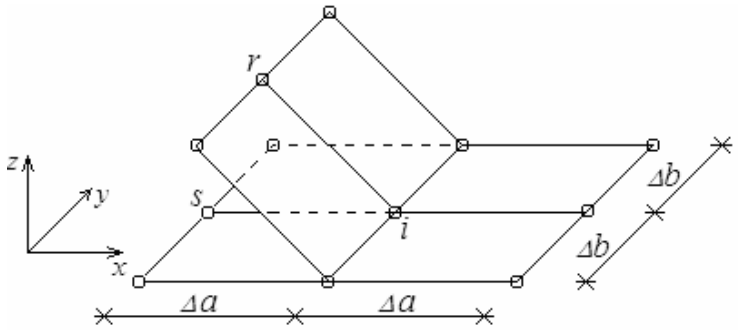

Fig. 10. Three-dimensional mesh scheme with eight-nodded elements in crack front area

The subscripts denote the corresponding nodes shown in Fig. 10. When the model is meshed using twenty-nodded finite elements (Fig. 11) the mode components of the strain energy release rate can be obtained as:

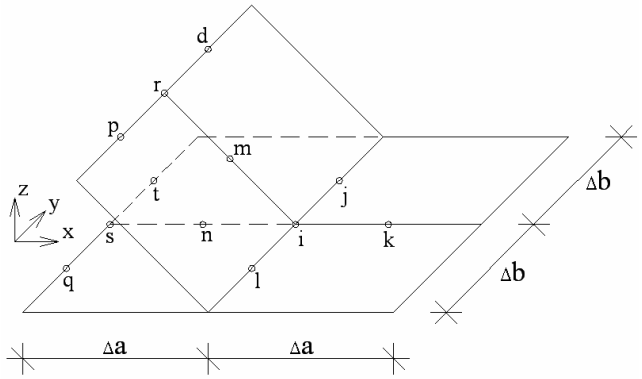

Fig. 11. Three-dimensional mesh scheme with twenty-nodded elements in crack front area

$$G_I = \frac{1}{2\Delta a\Delta b}\left[Z_i\left(w_r - w_s\right) + Z_k\left(w_m - w_n\right) + \frac{1}{2}Z_l\left(w_p - w_q\right) + \frac{1}{2}Z_j\left(w_d - w_t\right)\right], \tag{32}$$

$$G_{II} = \frac{1}{2\Delta a\Delta b}\left[X_i\left(u_r - u_s\right) + X_k\left(u_m - u_n\right) + \frac{1}{2}X_l\left(u_p - u_q\right) + \frac{1}{2}X_j\left(u_d - u_t\right)\right], \tag{33}$$

$$G_{II} = \frac{1}{2\Delta a\Delta b}\left[Y_i\left(v_r - v_s\right) + Y_k\left(v_m - v_n\right) + \frac{1}{2}Y_l\left(v_p - v_q\right) + \frac{1}{2}Y_j\left(v_d - v_t\right)\right]. \tag{34}$$

Another method for strain energy release rate calculation is the crack closure technique. The application of this technique requires two analyses by the finite element model. The first analysis which is performed just prior to crack growth yields the nodal forces at the crack tip. The crack advance is simulated in the second analysis by releasing the crack tip nodes. The second analysis provides the corresponding nodal displacement needed to calculate the strain energy release rate mode components. The crack closure technique assumes that the nodal forces, obtained in the first analysis, are forces needed to closure the crack. The work performed during the process of crack closure can

be calculated by multiplying one half of the nodal forces with the corresponding nodal displacements. The strain energy release rate mode components at node c in Fig. 8 can be obtained by the formulae:

$$G_I = \frac{1}{2\Delta l}\left(Y_c \delta v_c\right), \tag{35}$$

$$G_{II} = \frac{1}{2\Delta l}\left(X_c \delta u_c\right), \tag{36}$$

where δu and δv are the differences in the nodal displacement components. The mode components of the strain-energy release rate if eight-nodded elements are used (Fig. 9) can be defined as:

$$G_I = \frac{1}{2\Delta l}\left(Y_c \delta v_c + Y_d \delta v_d\right), \tag{37}$$

$$G_{II} = \frac{1}{2\Delta l}\left(X_c \delta u_c + X_d \delta u_d\right). \tag{38}$$

The strain energy release rate mode components for the 3-D crack problem shown in Fig. 10 can be expressed as:

$$G_I = \frac{1}{2\Delta a \Delta b}\left(Z_i \delta w_i\right), \tag{39}$$

$$G_{II} = \frac{1}{2\Delta a \Delta b}\left(X_i \delta u_i\right), \tag{40}$$

$$G_{III} = \frac{1}{2\Delta a \Delta b}\left(Y_i \delta v_i\right). \tag{41}$$

The node components of the strain energy release rate for a mesh developed using higher ordered elements (Fig. 11) can be calculated as:

$$G_I = \frac{1}{2\Delta a \Delta b}\left(Z_i \delta w_i + Z_k \delta w_k + Z_l \delta w_l + Z_j \delta w_j\right), \tag{42}$$

$$G_{II} = \frac{1}{2\Delta a \Delta b}\left(X_i \delta u_i + X_k \delta u_k + X_l \delta u_l + X_j \delta u_j\right), \tag{43}$$

$$G_{III} = \frac{1}{2\Delta a \Delta b}\left(Y_i \delta v_i + Y_k \delta v_k + Y_l \delta v_l + Y_j \delta v_j\right). \tag{44}$$

The total strain energy release rate G, is calculated from the mode components as:

$$G = G_I + G_{II} + G_{III}, \tag{45}$$

where $G_{III} = 0$ for the 2-D cases presented in Figs 8 and 9.

The virtual crack closure technique was used for solving a variety of fracture problems [46, 110, 111, 112]. Mode I, mode II, or mixed-mode I/II cracks were considered in most of the cases. 2-D finite element models were developed for this purpose.

The virtual crack closure technique was applied to analyze the strain energy release rate from pure mode I through various mixed-modes I/II up to pure mode II crack loading conditions in Refs [113, 114].

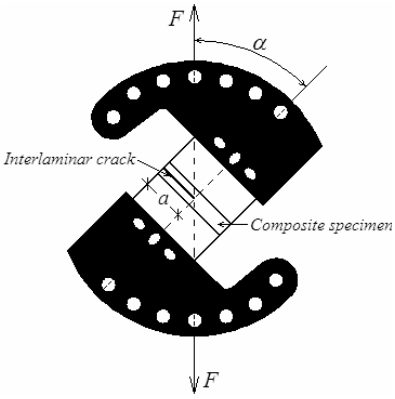

Fig. 12. Compact tension shear specimen

Interlaminar fracture behaviour of a glass/epoxy composite was studied using the compound version of the Compact Tension Shear (CTS) specimen (Fig. 12). The load F is applied by a special loading device under an arbitrary angle α with respect to the specimen. A full range of mixed-mode crack loading conditions can be achieved by changing angle α from pure mode I ($\alpha = 0$) through various mixed-mode I/II loadings ($0° < \alpha < 90°$) up to pure mode II ($\alpha = 90°$). The composite specimen (a strip with an initial interlaminar crack of length a) is glued into the end blocks which carry the applied loads. The basic advantage of the CTS test method is that all in-plane loading conditions can be achieved using only one type of specimen. The loading was applied using a constant displacement rate of 0.5 mm/min during the testing. The measured critical load at the crack growth initiation was used to calculate the strain energy release rate mode components by the virtual crack closure technique. 2-D finite element simulations were conducted of the CTS specimen for this purpose. The nodal force at the crack tip and the nodal displacements behind it generated by the finite element simulations were substituted in the equations of the virtual crack closure technique to obtain the separated strain

energy release rates. It was found that the critical strain energy release rate for pure mode II loading conditions was about 9 times higher than that for pure mode I loading. The calculation revealed also that the critical strain energy release rates for mixed-mode I/II loading conditions are between those for the pure modes. The results obtained for pure mode I and pure mode II loading conditions by the CTS specimen were compared with the results generated by the DCB (for mode I) and the ENF (for mode II), respectively. A mixed-mode I/II fracture criterion was formulated for the composite material under consideration on the basis of the CTS test results.

Fracture behaviour of composites can also be studied using micromechanical models [115]. In general, these models are based on assumptions for uniform distribution and periodic packing of the fibres. The concept of representative cell is widely applied in micromechanics. This concept is very convenient from computational point of view since the composite can be investigated by considering only a representative unit cell limited by the planes of symmetry. The unit cell is analyzed by the finite element method. The micromechanical models are suitable also for examination of the local details of the stress state of the composite. It should be mentioned, that these details can not be measured directly through experiments. However, the local stress field illustrates the reason and the pattern of the composite failure (for instance, the stress concentration and redistribution are crucial for the crack initiation and crack growth).

Although mode III interlaminar fracture behaviour has received comparatively less attention, some advance has been done for the last two decades [116, 117, 118, 119, 120, 121, 122, 123].

Becht and Gillespie proposed a mode III fracture test called the Crack Rail Shear (CRS) specimen. Design and analysis of the CRS test method is presented in Ref. [124]. The specimen geometry is shown in Fig. 13.

In general, the specimen configuration is similar to the two-rail shear test for characterization of the in-plane shear properties of continuous fibre reinforced composites. Kapton film placed symmetrically about the specimen midplane serves as the initial interlaminar crack. The following analytical expression for the strain energy release rate assuming a pure shear stress state and using a strength-of-materials approach was obtained:

$$G = \frac{F^2}{4L^2h}\left(\frac{b-1}{G'}\right), \tag{46}$$

where G' is the shear modulus, L, h, and b are the length, thickness of the strap section, and total thickness of the specimen, F is the applied load (Fig.

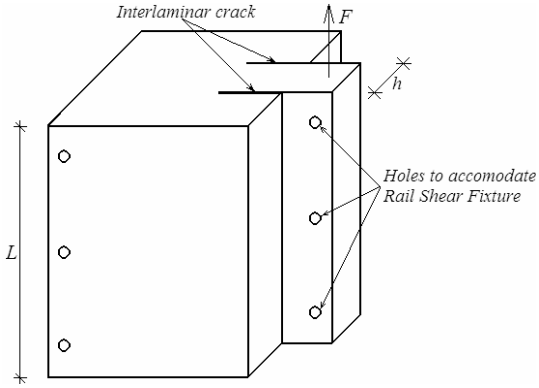

Fig. 13. Crack rail shear specimen.

13). The strain energy release rate was evaluated also using the compliance method.

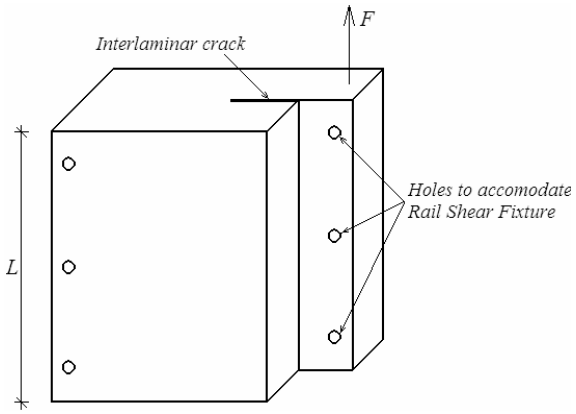

Fig. 14. Single crack rail shear specimen

Single crack CRS specimens were used to characterize the interlaminar mode III critical strain energy release rate of composites in Ref. [125]. The specimen geometry and loading are illustrated in Fig. 14. It is obvious, that the specimen is very similar to the double crack version of the CRS test shown in Fig. 13. A procedure was developed to determine the critical load value using experimental results. The fracture surface morphology was observed by a Scanning Electron Microscope upon completion of the experiments. Three-dimensional linear-elastic finite element analysis of the single crack CRS spec-

imen was carried-out. The strain energy release rate mode components were calculated by the crack closure technique.

The major drawback of the CRS test is the low compliance of the specimen. Another method for characterizing mode III interlaminar fracture toughness is the Split Cantilever Beam (SCB) specimen. Geometry and loading of the SCB is depicted in Fig. 15. It is obvious that the SCB is similar to the DCB specimen, except that the loading direction is parallel to the interlaminar crack plane.

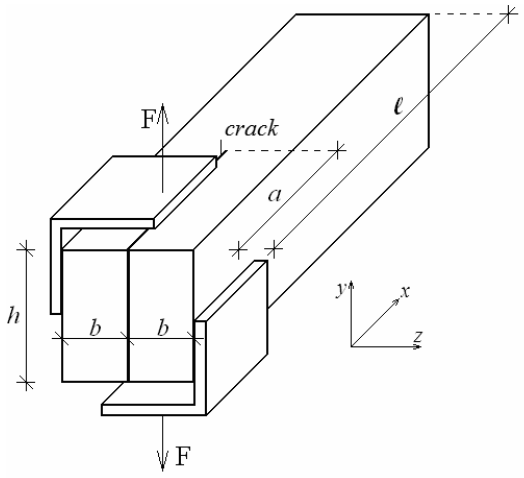

Fig. 15. Split cantilever beam specimen

SCB specimens were used by Donaldson for mode III interlaminar fracture characterization of fibre reinforced composites [121]. The unidirectional composite was bonded between two aluminium bars. The specimens contained initial interlaminar cracks of length a, located at their midplane. The crack arms were loaded in opposite directions at a constant displacement rate of 0.5 mm/min. Stable crack growth was achieved. Load-displacement diagrams recorded during the experiments were linear until crack growth occurred. Crack tip positions were monitored on the upper and the lower specimen surfaces throughout the test. It was found, that crack lengths on both specimen surfaces were almost equal. No plastic deformation occurred. The fracture toughness was studied in terms of the critical strain energy release rate. The effect of laminate thickness and beam depth were investigated. The calculated mode III fracture toughness was roughly double the mode II value and nine times the mode I value for the composite under consideration.

The SCB specimen was analyzed by Martin using linear-elastic fracture mechanics [122]. Also, experiments were conducted using SCB specimens manufactured by unidirectional glass/epoxy composites. The tests were carried-out under displacement control at a cross head rate of 0.5 mm/min. The onset of crack growth from the initial interlaminar crack was observed at the end of the linear part of the load-displacement plot recorded during the testing. The load-displacement plot 'returned' in the origin of the coordinate system after unloading for all tests. The crack surfaces of the specimen were examined using a scanning electron microscope after testing. Tangled fibres were observed in the central area of the crack front which was an indication that in this area interlaminar fracture was in mode III. However, shear hackles at the edge of the specimen caused by mode II fracture were found. Therefore, it was concluded that the SCB configuration is not a pure mode III interlaminar fracture test.

An improved mode III interlaminar fracture test for composites was developed in Ref. [123]. The test method uses a configuration similar to the SCB specimen. A special test jig was manufactured to ensure elimination of the unwanted mode II component at the edges of the crack of the crack front. The basic idea is that the mode II can be eliminated by reducing the bending moments at the crack front area to zero. The SCB composite specimen was bonded into a deep recess in high strength aluminium bars to apply the required loading pattern. Two forces were applied to each crack arm using a beam which was connected to the specimen at two suitably chosen positions. In this way, crack front area bending moments in the two arms were reduced to zero. The improved mode III test method was used to investigate interlaminar fracture behaviour of unidirectional carbon/epoxy composite. Initial cracks were formed by incorporating Teflon film at the midplane of each specimen. The tests were performed at a constant cross-head displacement rate of 0,5 mm/min. Six specimens were tested. Load-displacement plots were recorded for each test. In all cases the plots were linear to delamination crack growth onset. Very good repeatability of the experimental data was achieved. Fracture surfaces of the modified SCB specimens were examined by a scanning electron microscope. No mode II shear hackles were observed along the initial crack front position. It was found that in the area near the edge the resin was pulled away from the fibres. In the central area of the specimen the fibres were partially covered by the resin. This variation in fracture surface characteristics was attributed to the non-uniform distribution of the strain energy release rate along the crack front. Three-dimensional linear-elastic finite element simulations were performed in order to evaluate the strain energy release rate in the improved version of the SCB specimen. The mode components of the strain

energy release rate were calculated via the finite element model using the virtual crack closure technique. It was found that the delamination crack growth was essentially pure mode III. The effect of composite specimen width on the mode III inretlaminar fracture was studied. It was found, that the strain energy release rate distribution is more uniform along the crack front in narrow specimens.

Another modification of the SCB specimen was developed in Ref. [126]. Two forces are applied directly to each crack arm of the SCB specimen, as illustrated in Fig. 16 in order to achieve pure mode III crack loading conditions.

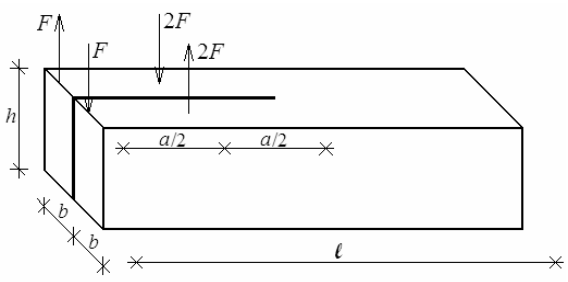

Fig. 16. Modified split cantilever beam specimen

For this purpose, a pair of identical grips is used to load the crack arms. The complex loading configuration is necessary to reduce the mode II component by eliminating the bending moments in the delamination front area of the two crack arms (i.e., the bending moments in the delamination front area induced by the two forces are equal and opposite). The modified SCB specimen was used to investigate mode III delamination fracture behaviour of carbon fibre reinforced epoxy composite. The experimentally obtained loads-displacement diagrams were linear up to the crack growth initiation point. The delamination fracture surfaces were studied by a scanning electron microscope. Three dimensional finite element simulations of the SCB were carried-out. Linear-elastic fracture mechanics was used. The virtual crack closure technique was applied to calculate the separated mode components of the strain energy release rate along the delamination crack front. It was found that the mode III component dominated the fracture (a small amount of mode II components was present only in a zone near the edges of the specimen).

The modified SCB test method was used to investigate the influence of low temperatures on the mode III interlaminar fracture behaviour of glass fibre reinforced polymer woven laminates in Ref. [127]. The investigation

was motivated by the fact that laminated composites have been used recently as structural members at low temperature environments. The basis for the investigated composite is the glass fabric of E-glass. The matrix is a bisphenol-A epoxy resin. Teflon film was inserted along the edge of the laminate in order to provide the initial midplane delamination crack. The SCB specimens were cut from the woven glass-epoxy laminates. The length of the initial crack was chosen to be five times the height of the SCB cross-section. Mode III delamination fracture tests were carried-out using a rig consisting of two steel plates with adjustable loading positions to accommodate SCB specimens with different initial crack lengths. Schematic of one loading plate and specimen is depicted in Fig. 17.

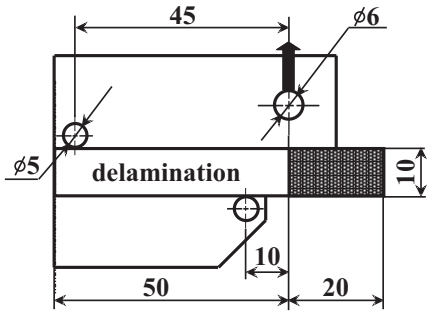

Fig. 17. Loading of one half of the modified split cantilever beam specimen

The modified SCB test set-up is shown in Fig. 18. The potential for mode I fracture was eliminated by constraining the loading plates with rigid clamps, attached with minimum clamping pressure.

All tests were conducted using a cross-head speed of 0.6 mm/min. The resulted load-displacement diagram was recorded automatically during the testing. The fracture surfaces were examined using a scanning electron microscope in order to verify the failure mechanisms.

A micrograph of the central section of the delamination fracture surface is shown in Fig. 19. It can be observed that the mode II shear hackles are relatively limited in this section, which is an indication that the fracture is mode III dominated. An area of the fracture surface near the edge of the SCB specimen is reported in Fig. 20.

Numerous mode II shear hackles can be observed, which is evidence that in this area the interlaminar crack grows under mixed-mode I/II conditions. A three-dimensional finite element model of the SCB specimen was set-up in order to analyze the distribution of the strain energy release rate

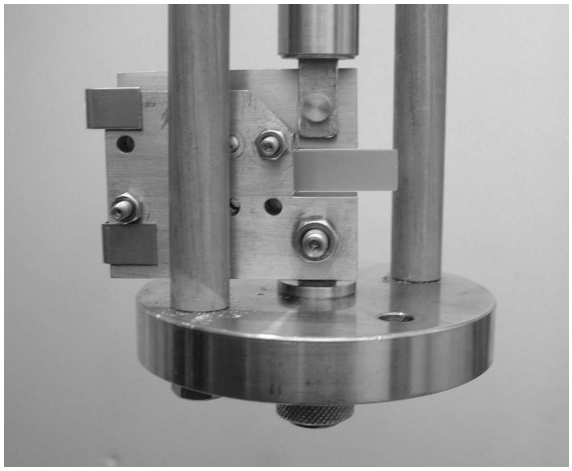

Fig. 18. The modified split cantilever beam specimen set-up

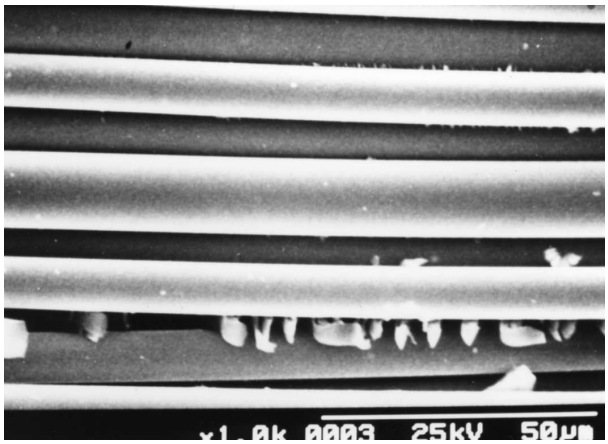

Fig. 19. Scanning electron microscope fractograph of the central zone of the delamination fracture surface

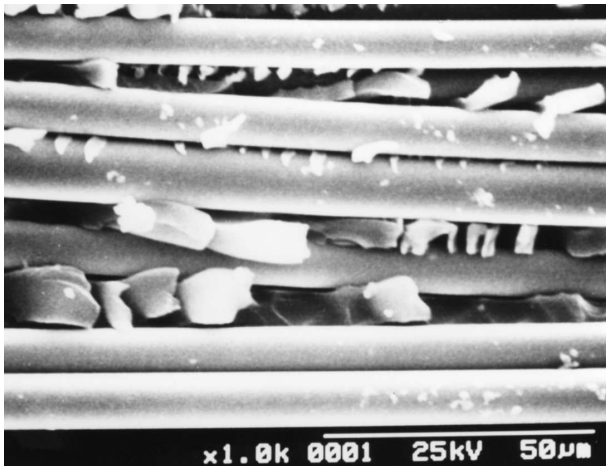

Fig. 20. Scanning electron microscope fractograph of the free edge zone of the delamination fracture surface

mode components along the interlaminar crack front. The numerical model was based on the geometry and the dimensions of the specimen used in the experimental investigation. The composite was modelled as a linear-elastic orthotropic material. The strain energy release rate was calculated using the virtual crack closure technique. The results obtained were verified by the crack closure technique. The stress intensity factors along the delamination crack front were evaluated using a solution proposed by Sih et al. [128]. The following relationships were applied:

$$G_{IIC} = \pi K_{IIC}^2 \frac{a_{11}}{\sqrt{2}} \left(\sqrt{\frac{a_{33}}{a_{11}}} + \frac{2a_{13} + a_{55}}{2a_{11}} \right)^{\frac{1}{2}}, \tag{47}$$

$$G_{IIIC} = \pi K_{IIIC}^2 \frac{1}{2\sqrt{c_{44} c_{66}}}, \tag{48}$$

$$a_{11} = \frac{1}{E_x}, \quad a_{13} = -\frac{\nu_{xz}}{E_x}, \quad a_{33} = \frac{1}{E_z}, \quad a_{55} = \frac{1}{G_{zx}}, \tag{49}$$

$$c_{44} = \frac{1}{a_{44}}, \quad c_{66} = \frac{1}{a_{66}}, \tag{50}$$

$$a_{44} = \frac{1}{G_{yz}}, \quad a_{66} = \frac{1}{G_{xy}}, \tag{51}$$

where E_x, E_y, E_z, G_{xy}, G_{yz}, and G_{zx} are the elastic properties of the composite material, G_{II} and G_{III} are the mode II and mode III components of the strain

energy release rate, K_{II} and K_{III} are the mode II and mode III stress intensity factors, respectively.

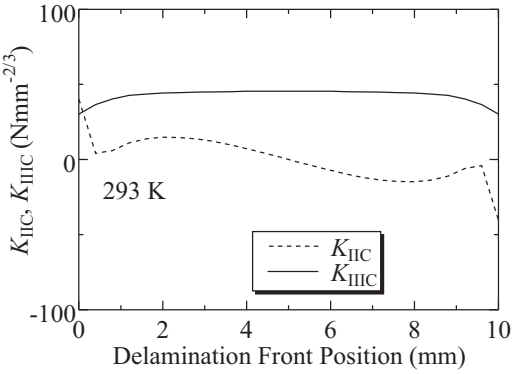

Fig. 21. Distribution of the critical stress intensity factors along the delamination crack front

It should be noted that the mode I stress intensity factor is zero, because in the modified version of the SCB specimen the fracture occurs under mixed-mode II/III crack loading conditions. Formulae (47) and (48) were applied at each node along the delamination front in order to obtain the distribution of the stress intensity factors (once the mode components of the strain energy release rate were calculated by the virtual crack closure technique). The distribution of K_{II} and K_{III} is reported in Fig. 21.

REFERENCES

[1] Shahvooz, B., S. Boy, T. Baseheart. Flexural Strengthening of Four 76–Year-old T-Beams with Various Fiber-Reinforced Polymer Systems: Testing and Analysis. *ACI Structural Journal,* **99** (2002), No. **5**, 681–691.

[2] Sheikh, S., D. De Rose, J. Mardukhi. Retrofitting of Concrete Structures for Shear and Flexure with Fiber-Reinforced Polymers. *ACI Structural Journal*, **99** (2002), No. **4**, 451–459.

[3] Arduiri, M., A. Nanni, M. Romagnolo. Performance of Decommissioned Reinforced Concrete Girders Strengthened with Fiber-Reinforced Polymer Laminates. *ACI Structural Journal*, **99** (2002), No. **5**, 652–659.

[4] Sheikh, S., G. Yan. Seismic Behaviour of Concrete Columns Confined with Steel and Fiber-Reinforced Polymers. *ACI Structural Journal*, **99** (2002), No. 1, 72–80.

[5] Saadatmanesh, H., M. Ehsani. Fiber Composite Bar for Reinforced Concrete Construction. *Journal of Composite Materials*, **25** (1991), No. 2, 188–203.

[6] Chaalal, O., M. Shahawy, M. Hassan. Performance of Reinforced Concrete T-girders Strengthened with Carbon Fiber Reinforced Polymer Fabric. *ACI Structural Journal*, **99** (2002), No. **3**, 335–343.

[7] Shahwy, M., O. Chaalal, T. Beitelman, A. El-Saad. Flexural Strengthening with Carbon Fiber Reinforced Polymer Composites of Preloaded Full Scale Girders. *ACI Structural Journal*, **98** (2001), No. **5**, 737–742.

[8] Yeong-Soo, S., C. Lee. Flexural Behaviour of Reinforced Concrete Beams Strengthened with Carbon Fiber Reinforced Polymer Laminates at Different Levels of Sustaining Load. *ACI Structural Journal*, **99** (2003), No. **3**, 231–239.

[9] Dinev, D. Investigation of Flexural Behaviour of Structures Strengthened by Composite Materials, Ph. D. – Thesis, UACEG-Sofia, 2006 (in Bulgarian).

[10] Phares, B. M., T. J. Wipf, F. W. Klaiber, A. Abu-Hawash, Yoon-Si Lee. Strengthening of Steel Grider Bridges using Frp. In: Proceedings of the 2003 Mid-Continent Transportation Research Symposium, Iowa, Ames, August 2003.

[11] Wipf, T. J., B. M. Phares, F. W. Klaiber, Yoon-Si Lee. Evaluation of Post-tensioned Strengthened Steel Girder Bridge using Frp Bars, Final Report, Center for Transportation Research and Education, Iowa State University, November 2003.

[12] Dulevsky, E. M., L. D. Georgiev. Strengthening of Steel Members under Bending by Means of Cfrp Strips, International Conference on Bridges, Croatia, Dubrovnik, 21–24. 06. 2006.

[13] Tumialan, J., A. Morbin, F. Michelli, A. Nanni. Flexural Strengthening of URM Walls with FRP Laminates, ICCI 2002, 11–23.

[14] Albert, L., A. Elwi, J. Cheng. Strenthening of Unreinforced Masonry Walls using FRPs. *ASCE*, **5** (1996), No. **2**, 76–84.

[15] Tumialan, J., N. Galati, A. Nanni. Fiber-Reinforced Polymer Strengthening of Unreinforced Masonry Walls Subject to Out-of Plane Loads. *ACI Structural Journal*, **99** (2003), No. **4**, 321–329.

[16] Busschen, A. Micromechanical Modelling of Uni-directional Glass Fiber Reinforced Polyester: Effect of Matrix Shrinkage, In: Proc. Euromech Colloquim 269, (Ed. A. Vautrin), France, St. Etienne, 1991, 1–8.

[17] Zhang, L., L. Ernst. Implementation of a Nonlinear Viscoelastic Theory, In: Finite Elements in Engineering and Science, Rotterdam, Balkema, 1997, 473–486.

[18] Zhang, L., L. Ernst, H. Brouwer. Transverse Behaviour of a Unidirectional Composite (Glass Fiber Reinforced Unsaturated Polyester). Part I. Influence of Fiber Packing Geometry. *Mechanics of Materials*, **27** (1998), No. **1**, 13–36.

[19] Zhang, L., L. Ernst, H. Brouwer. Transverse Behaviour of a Unidirectional Composite (Glass Fibre Reinforced Unsaturated Polyester). Part II. Influence of Shrinkage Strains. *Mechanics of Materials*, **27** (1998), No. **1**, **37**–61.

[20] Bushen, A., A. Selvadurai. Mechanics of the Segmentation of an Embedded Fiber, part I: Experimental Investigations. *Journal of Applied Mechanics*, **62** (1995), No. **1**, 87–97.

[21] Bushen, A., A. Selvadurai. Mechanics of the Segmentation of an Embeded Fiber, part II: Computational Modelling and Comparisons. *Journal of Applied Mechanics*, **62** (1995), No. **1**, 98–107.

[22] Kalinin, I. L. Surface of Carbon Fibres, its Modification and Influence on the Fracture of Carbon Fibre Plastics, In: Fracture of Composite Materials, Riga, Zinatne, 1979, 221–230 (in Russian).

[23] Kalinin, I. L. Cracks and Defects in Carbon Fibres, In: Strength and fracture of composite materials, Riga, Zinatne, 1983, 48–56 (in Russian).

[24] Composite Materials: Handbook, Editors: V. V. Vasileva, U. M. Tarnopolsky. – M., Mashinostroene, 1990, 512 p. (in Russian).

[25] Composite Materials: Handbook, Editor: D. M. Karpinos. – Kiev, Naukova Dumka, 1985, p. 592. (in Russian).

[26] Deformation, Fracture and Strength of Polymer Composite Materials, Report, Institute of Mechanics, M., MGU 'Lomonosov', 1988, 124 p. (in Russian).

[27] Perminov, V. P., A. M. Votinov, A. I. Tarakanov. Some Problems of Assessment of Load Bearing Capacity of Carbon Composite Structures, In: Proceedings of the 4-th School of Structural Design. – Tbilisi, 1983. 26 p. (in Russian).

[28] Fracture of Composite Structures, Editors: V. P. Tamuj, V. D. Protasov. – Riga, Zinatne, 1986, 264 p. (in Russian).

[29] Sokolkin, U. V., A. A. Tashkinov. Mechanics of Deformation and Fracture of Inhomogeneous Solids, M., Nauka, 1984, 116 p. (in Russian).

[30] Sokolkin, U. V., A. A. Tashkinov. Statistical Models of Deformation and Fracture of Composites. *Mechanics of Composite Materials,* **21** (1984), No. **5**, 844–849.

[31] Tankeeva, M. G., A. A. Tashkinov, U. V. Sokolkin, A. M. Postnih. Assessment of Composite Structures Strength, In: Proceedings of UO AN USSR, Sverdlovsk, 1989, 79 p. (in Russian).

[32] Griffitz, A. A. The Phenomena of Rupture and Flow in Solids. *Philosophical Transactions of the Royal Society*, **221A** (1920), 163–198.

[33] Westergaard, H. M. Bearing Pressures and Cracks. Transactions of the ASME, Series E. *Journal of Applied Mechanics*, **61**, (1939), A49–A53.

[34] Tada, H., P. C. Paris, G. R. Irwin. The Stress Analysis of Cracks. Handbook, PA, Hellertown, Del Research Corporation, 1973.

[35] Parvanova, S. Application of the Singular Field Approach at the Dual Boundary Element Method, Annual of The University of Architecture, Civil Engineering and Geodesy, **XLIII** vol., fasc. **V**, 2006–2007, (in Bulgarian).

[36] Parvanova, S., G. Gospodinov. A Dual Boundary Element Procedure for Analysis of Fracture in Concrete. *Journal of Theoretical and Applied Mechanics*, (2007), No. **1** , 65–80.

[37] Parvanova, S. Calculation of Stress Intensity Factors Based on Force-displacement Curve Using Element Free Galerkin Method. *Journal of Theoretical and Applied Mechanics*, (2012), No. **1**, 23–40.

[38] Kerelezova, I. G. Numerical Determination of the Crack Path in Concrete Beams, Annual of The University of Architecture, Civil Engineering and Geodesy, **XL** vol., fasc. **VI**, 2002–2003 (in Bulgarian).

[39] Gospodinov G., P. Drakaliev, I. Kerelzova. A Singular Boundary Element Method for the General Corner Case, In: Anniversary Scientific Conference 50 Years Faculty of Hydrotechnics of The University of Architecture, Civil Engineering and Geodesy, 6–8 Oct. 1999, V-113–V-119.

[40] Kerelezova, I., G. Gospodinov. A Boundary Elements Numerical Procedure Applied to Effective Crack Approach, Annual of The University of Architecture, Civil Engineering and Geodesy, **XLI** vol., fasc. **I**, 2004–2005.

[41] Rice, J. R. A Path Independent Integral and the Approximate Analysis of Strain Concentration by Notches and Cracks. *Journal of Applied Mechanics*, **35** (1968), No. **1**, 27–39.

[42] Hutchinson, J. W. Singular Behaviour at the End of a Tensile Crack Tip in a Hardening Material. *Journal of the Mechanics and Physics of Solids*, **16** (1968), No. **1**, 13–31.

[43] Rice, J. R., G. F. Rosengren. Plane Strain Deformation Near a Crack Tip in a Power-law Hardening Material. *Journal of the Mechanics and Physics of Solids*, **16** (1968), No. **1**, 1–12.

[44] Hojo, M., S. Ochiai, N. Joyama, J. Takahashi. Fracture Mechanism of Cross-ply Carbon/carbon Composites. *Advanced Composite Materials*, **5** (1996), No. **2,** 99–117.

[45] Kawada, H., M. Matsumori, H. Omata, T. Uruno, J. Hiramoto, I. Hayashi. Evaluation of Fracture Toughness in C/C Composites. *Trans. Japan Soc. Engrs.* **60–572A** (1994), 978–983.

[46] Rikards, R., A. Korjakin, F. Buchholz, H. Wang, A. Bledzki, G. Wacker. Interlanimar Fracture Toughness of GFRP Influenced by Fiber Surface Treatment. *Journal of Composite materials*, **32 (**1998), No. **17**, 1528–1559.

[47] Zhao, S., M. Gadke, R. Prinz. Mode I Delamination Behaviour of Carbon/epoxy Composites. *J. Reinf. Plast. And Comp.*, **14** (1995), No. **4**, 804–826.

[48] Davies, P., C. Moulin, H. Kausch. Measurement of G_{IC} in Carbon/epoxy Composites. *Comp. Sci. And Technol.*, **39 (**1990), No. **2**, 193–206.

[49] Zhou J., He T. On the Analysis of End-notched Flexure Specimen for Measuring Fracture Toughness of Composite Materials. *Comp. Sci. Technol.*, **50**, (1994), No. **2**, 209–213.

[50] Hojo, M., K. Kageyama, K. Tanaka. Prestandartization Study on Mode I Interlaminar Fracture Toughness Test for CFRP in Japan. *Composites*, **26**, (1995), No. **2**, 243–255.

[51] Robinson, P., D. Q. Song. A Modified DCB Specimen for Mode I Testing of Multidirectional Laminates. *J. Compos. Mater.*, **26** (1992), No. **11**, 1554–1577.

[52] Shokrieh, M.M., M. Heidari-Rarani. Effect of Stacking Sequence on R-curve Behaviour of Glass/epoxy DCB Laminates with $0^\circ//0^\circ$ Crack Interface. *Materials Science and Engineering*, **529 (**2011), No. **2**, 265–269.

[53] Xiannian, S., D. K. Michael, K. Wood, L. Tong. A Parametric Study on the Design of Stitched Laminated DCB Specimens. *Composite Structures*, **75** (2006), No. **1**, 72–78.

[54] Gong X. J., A. Hurez, G. Verchery. On the Determination of Delamination Toughness by Using Multidirectional DCB Specimens. *Polymer Testing*, **29** (2010), No. **6**, 658–666.

[55] Yutaka, I., K. Nakane, N. Watanabe. DCB Test Simulation of Stitched CFRP Laminates using Interlaminar Tension Test Results. *Composites Science and Technology*, **69** (2009), No. **14**, 2315–2322.

[56] Tomohiro, Y., T. Ogasawara, T. Aoki. Correction Method for Evaluation of Interfacial Fracture Toughness of DCB, ENF and MMB Specimens with Residual Thermal Stresses. *Composites Science and Technology*, **68** (2008), No. **3–4**, 760–767.

[57] Brunner, A. J. Experimental Aspects of Mode I and Mode II Fracture Toughness Testing of Fiber-reinforced Polymer-matrix Composites. *Comput. Methods. Appl. Mech. Eng.*, **185 (**2009), No. **3,** 161–172.

[58] Rikards, R. Interlaminar Fracture Behaviour of Laminated Composites. *Comput. Struct.*, **76** (2010), No. **2**, 11–18.

[59] ASTM D 5528-94a, Standard Test Method for Mode I Interlaminar Fracture Toughness of Unidirectional Fiber-reinforced Polymer Matrix Composites, *Annual Book of ASTM Standards*, 15.03, Am. Soc. For Testing and Materials, 2010.

[60] ASTM D 6115-97, Standard Test Method for Mode I Fatigue Delamination Growth Onset of Unidirectional Fiber-reinforced Polymer Matrix Composites, *Annual Book of ASTM Standards,* 15.03, Am. Soc. for Testing and Materials, 2010.

[61] Asp, L. E., A. Sjogren, E. S. Greenhalgh. Delamination Growth and Thresholds in a Carbon/epoxy Composite under Fatigue Loading. *J. Compos. Technol. Res.*, **23** (2010), No. **2**, 55–68.

[62] Jain, L., Y. Mai. On the Effect of Stitching on Mode I Delamination Toughness of Laminated Composites. *Comp. Sci. and Technology*, **51** (1994), No. **4**, 331–345.

[63] Shindo, Y., K. Horiguchi K., R. Wang R., H. Kudo. Double Cantilever Beam Measurements of Cryogenic Mode I Interlaminar Fracture Toughness of Glass-cloth/epoxy Laminates. *ASME Journal of Engineering Materials and Technology,* **123** (2001), No. **6**, 191–197.

[64] Humer, K., E. K. Tashegg, R. Platschka, H. W. Weber. Acoustic Emission Studies on Irradiated Plastic-Coper Interfaces in Mode I at Room Temperature and 77K. *Adv. Cryog. Eng.* **42** (1996), No. **2**, 51–56.

[65] Point, N., E. Sacco. Delamination of Beams: an Application to tha DCB Specimen. *International Journal of Fracture,* **79 (**1996), No. **4**, 225–247.

[66] Choi, N. S., A. J. Kinloch, J. G. Williams. Delamination Fracture of Multidirectional Carbon-fibre/epopxy Composite under Mode I, Mode II and Mixed-mode I/II Loading. *Journal of Composite Materials*, **32** (1997), No. **5**, 1808–1835.

[67] Ozdil, F., L. A. Carlsson, P. Davies. Beam Analysis of Angle-ply Laminated End-notched Flexure Specimens. *Composite Science and Technology* **58** (1998), No. **4**, 1929–1938.

[68] Bullions, T. A., R. H. Mehta, B. Tan, J. E. McGrath, D. Kranbuehl, A. C. Loos. Mode I and Mode II Fracture Toughness of High-performance 3000 g mole^{-1} Reactive Ply(Etherimide)/carbon Fibre Composites. *Composites Part A: Applied Science and Manufacturing*, **30** (1999), No. **3**, 153–162.

[69] Broek, D. Elementary Engineering Fracture Mechanics, 4-th ed., The Netherlands, Dordrecht: Marinus Nijhoff Publishers, 1986.

[70] Davidson, B., R. Kruger, M. Konig. Effect of Stacking Sequence on Energy Release Rate Distributions in Multi-dimensional DCB and ENF Specimens. *Eng. Fracture Mech.*, **55** (1996), No. **5,** 557–575.

[71] Chengye, F., P. Y. Ben Jar, J. J. Roger Cheng. Revisit the Analysis of End-notched-flexure (ENF) Specimen. *Composites Science and Technology*, **66** (2006), No. **10**, 1497–1498.

[72] Pankow, M., A. Salvi, A. M. Waas, C. F. Yen, S. Ghiorse. Resistance to Delamination of 3D Woven Textile Composites Evaluated using End Notch Flexure Tests: Experimental Results. *Composites Part A: Applied Science and Manufacturing*, **42** (2011), No. **10**, 1463–1476.

[73] Pankow, M., A. M. Waas, C. F. Yen, S. Ghiorse. Resistance to Delamination of 3D Woven Textile Composites Evaluated using End Notch Flexure Tests: Cohesive Zone Based Computational Results. *Composites Part A: Applied Science and Manufacturing*, **42** (2011), No. **12**, 1863–1872.

[74] Tomohiro Y., T. Ogasawara, T. Aoki. Correction Method for Evaluation of Interfacial Fracture Toughness of DCB, ENF and MMB Specimens with Residual Thermal Stresses. *Composites Science and Technology*, **68** (2008)**,** No. **3–4**, 760–767.

[75] de Moura M. F. S. F., A. B. de Morais. Equivalent Crack Based Analyses of ENF and ELS Tests. *Engineering Fracture Mechanics*, **75** (2008), No. **9**, 2584–2596.

[76] Todo M., P. Y. B. Jar, K. Takahashi. Initiation of a Mode-II Interlaminar Crack from an Insert Film in the End-notched Flexure Composite Specimen. *Composites Science and Technology*, **60** (2000), No. **2**, 263–272.

[77] Davies, P., G. D. Sims, B. R. K. Blackman, A. J. Brunner, K. Kageyama, M. Hojo, K. Tanaka, G. Murri, C. Rousseau, B. Gieseke., R. H. Martin. Comparison of Test Configurations for Determination of Mode II Interlaminar Fracture Toughness Results from International Collaborative Test Program. *Plastics, Rubber Compos*, **28** (1999), No. **9**, 432–437.

[78] Davies, P., B. R. K. Blackman, A. J. Brunner. Standard Test Methods for Delamination Resistance of Composite Materials: Current Status. *Appl. Compos. Mater.* **5** (1998), No. **2**, 345–364.

[79] Brunner, A. J. Experimental Aspects of Mode I and Mode II Fracture Toughness Testing of Fiber-reinforced Polymer-matrix Composites. *Comput. Methods Appl. Mech.*, **185** (2000), No. **4**, 161–172.

[80] Shi, Y. B., D. Hull, J. N. Price. Mode II Fracture of Angled Laminate Interfaces. *Comps. Sci. Technol.* **47** (1993), No. **2**, 173–184.

[81] Horiguchi, K.,Y. Shindo, H. Kudo, S. Kumagai. End-notched Flexure Testing and Analysis of Mode II Interlaminar Fracture Behaviour of Glass-cloth/epoxy Laminates at Cryogenic Temperatures. *Journal of Composites, Technology & Research*, **24** (2002), No. **4**, 239–245.

[82] Davies, P., P. Casari, L. A. Carlsson. Influence of Fibre Volume Fraction on Mode II Interlaminar Fracture Toughness of Glass/epoxy using 4ENF Specimen. *Composite Science and Technology*, **65** (2005), No. **3,** 295–300.

[83] Davies, P. Influence of ENF Specimen Geometry on the Mode II Delamination Resistance of Carbon/peek. *Journal of Thermoplastic Composite Materials*, **10** (1997), No. **4**, 35–49.

[84] Hojo, M., S. Matsuda, B. Fiedler, T. Kawada, K. Moriya, S. Ochiai, H. Aoyama. Mode I and Mode II Dalamination Fatigue Crack Growth Behaviour of Alumina Fibre/epoxy Laminates in Liquid Nitrogen. *International Journal of Fatigue*, **24** (2002), No. **2**, 109–118.

[85] Mollón, V., J. Bonhomme, J. Viña, A. Argüelles. Theoretical and Experimental Analysis of Carbon Epoxy Asymmetric DCB Specimens to Characterize Mixed Mode Fracture Toughness. *Polymer Testing*, **29** (2010), No. **6**, 766–770.

[86] Mollón, V., J. Bonhomme, J. Viña, A. Argüelles. Mixed Mode Fracture Toughness: An Empirical Formulation for Determination in Asymmetric DCB Specimens. *Engineering Structures*, **32** (2010), No. **11**, 3699–3703.

[87] Mollón, V., J. Viña, A. Argüelles, J. Bonhomme, I. Viña. Influence of the Mode Mixity Ratio and Test Procedures on the Total Energy Release Rate in Carbon-Epoxy Laminates. *Procedia Engineering*, **10** (2011), No. **2**, 953–958.

[88] Prombut, P., L. Michel, F. Lachaud, J. J. Barrau. Delamination of Multidirectional Composite Laminates at $0^\circ/\theta^\circ$ PLY Interfaces. *Engineering Fracture Mechanics,* **73** (2006), No. **16**, 2427–2442.

[89] Datla, N. V., J. Ulicny, B. Carlson, M. Papini, J.K. Spelt. Mixed-mode Fracture Behaviour of Degraded Toughened Epoxy Adhesive Joints. *International Journal of Adhesion and Adhesives*, **31** (2011), No. **2**, 88–96.

[90] Mollón, V., J. Bonhomme, J. Viña, A. Argüelles, A. Fernández-Canteli. Influence of the Principal Tensile Stresses on Delamination Fracture Mechanisms and Their Associated Morphology for Different Loading Modes in Carbon/epoxy Composites. *Composites Part B: Engineering*, In Press, Corrected Proof, Available online 8 August 2011.

[91] Vellinga, W. P., Al. Fedorov, J. T. De Hosson. Residual Stress Pinning of Delamination Fronts on Polymer–metal Interfaces. *Thin Solid Films*, **517** (2008), No. **2**, 841–847.

[92] Blackman, B. R. K., A.J. Brunner, P. Davies. Delamination Fracture of Continuous Fibre Composites: Mixed-mode Fracture. *European Structural Integrity Society*, **28** (2001), 335–359.

[93] Khaled, S., Farid Taheri. The Strain Energy Release Rates in Adhesively Bonded Balanced and Unbalanced Specimens and Lap Joints. *International Journal of Solids and Structures*, **45** (2008), No. **25–26**, 6284–6300.

[94] Ben, W. K., A. H. Mayer. Influence of Fiber Direction and Mixed-mode Ratio on Delamination Fracture Toughness of Carbon/epoxy Laminates. *Composites Science and Technology*, **63** (2003), No. **5**, 695–713.

[95] de Moura, M.F.S.F., J.M.Q. Oliveira, J.J.L. Morais, N. Dourado. Mixed-mode (I + II) Fracture Characterization of Wood Bonded Joints. *Construction and Building Materials*, **25** (2011), No. **4**, 1956–1962.

[96] Ducept, F., P. Davies, D. Gamby. An Experimental Study to Validate Tests Used to Determine Mixed Mode Failure Criteria of Glass/epoxy Composites. *Composites Part A: Applied Science and Manufacturing*, **28** (1997), No. **8**, 719–729.

[97] Shindo, Y., F. Narita, S. Takahashi, T. Sato, T. Takeda. Analysis of Mixed-mode Interlaminar Fracture and Damage Behaviour of GFRP Woven Laminates at Cryogenic Temperatures. *Cryogenics*, **49** (2009), No. **2**, 80–83.

[98] Pereira, A.B., A.B. de Morais. Mixed Mode I + II Interlaminar Fracture of Glass/epoxy Multidirectional Laminates – Part 2: Experiments. *Composites Science and Technology*, **66** (2006), No. **13**, 1896-1902.

[99] Rugg, K.L, B.N. Cox, R. Massabò. Mixed Mode Delamination of Polymer Composite Laminates Reinforced through the Thickness by z-fibres. *Composites Part A: Applied Science and Manufacturing*, **33** (2002), No. **2**, 177–190.

[100] Shindo, Y., M. Miura, T. Takeda, N. Saito, F. Narita. Cryogenic Delamination Growth in Woven Glass/epoxy Composite Laminates under Mixed-mode I/II Fatigue Loading. *Composites Science and Technology*, **71** (2011), No. **5**, 647–652.

[101] Jagan, U., P. S. Chauhan, P. Venkitanarayanan. Energy Release Rate for Interlaminar Cracks in Graded Laminates. *Composites Science and Technology*, **68** (2008), No. **6**, 1480–1488.

[102] Kenane M., M.L. Benzeggagh. Mixed-mode Delamination Fracture Toughness of Unidirectional Glass/epoxy Composites. *Composites Part B: Engineering*, **42** (2011), No. **3**, 367–375.

[103] Reeder, J. R., Jr. J. H. Crews. The Mixed-mode Bending Method for Delamination Testing. *AIAA J.*, **28** (1990), No. **7,** 1270–1276.

[104] Reeder, J. R., Jr. J. H. Crews. Redesign of the Mixed-mode Bending Delamination Test to Reduce Nonlinear Effects. *J. Comps. Technol. Res.*, **14** (1992), No. **1**, 12–19.

[105] Asp, L. E., A. Sjogren, E. S. Greenhalgh. Delamination Growth and Thresholds in a Carbon/epoxy Composite under Cyclic Loading. *Journal of Composites Technology and Research*, **23** (2001), No. **2**, 55–68.

[106] Sjogren, A., L. E. Asp. Effects of Temperature on Delamination Growth in a Carbon/epoxy Composite. *International Journal of Fatigue* **24** (2002), No. **1**, 79–184.

[107] Ribicki, E. F., M. F. Kanninen. A Finite Element Calculation of Stress Intensity Factors by a Modified Crack Closure Integral. *Eng.Fract. Mech.*, **9** (1977), No. **2**, 931–938.

[108] Raju, I. S. Calculation of Strain-energy Released Rates with Higher Order and Singular Finite Elements. *Eng. Fract. Mech.,* **28** (1987), No. **3**, 251–274.

[109] Shivakumar, K. N., P. W. Tan, Jr. J. C. Newman. A Virtual Crack-closure Technique for Calculating Stress Intensity Factors for Cracked Three Dimensional Bodies. *Int.J. Fract.*, **36** (1988), No. **3**, R43–R50.

[110] Rikards, R., F. G. Bucholz, H. Wang. Finite Element Analysis of Delamination Cracks in Bending of Cross-ply Laminates. *Mech. Comp. Mater. and Struct.*, **2** (1995), No. **4**, 281–294.

[111] Davidson, B. D., V. A. Sundararaman. A Single Leg Bending Test for Interfacial Fracture Toughness Determination. *Int.J. Fract.*, **78** (1996), No. **3**, 193–210.

[112] Korjakin, A., R. Rikards, F. G. Buchholz, H. Wang H., A. Bledzki, A. Kessler. Comparative Study of Interlaminar Fracture Toughness of GFRP with Different Fiber Surface Treatments. *Polym. Compos.*, **19** (1998), No. **4**, 793–806.

[113] Rikards, R., F. G. Bucholz, H. Wang, A. K. Bledzki, A. Korjakin, H. A. Richard. Investigation of Mixed Mode I/II Interlaminar Fracture Toughness of Laminated Composites by using a CTS Type Specimen. *Engineering Fracture Mechanics* **61** (1998), No. **3**, 325–342.

[114] Rikards, R. Interlaminar Fracture Behaviour of Laminated Composites. *Computer and Structures*, **76** (2000), No. **5**, 11–18.

[115] Bakulin, V. N., A. A. Rassoha. Finite Elements Method and Holographic Interferometery in Mechanics of Composites, – M.: Mashinostroene, 1987, 312 p. (in Russian).

[116] Marat-Mendes, R., M. de Freitas. Characterisation of the Edge Crack Torsion (ECT) Test for the Measurement of the Mode III Interlaminar Fracture Toughness. *Engineering Fracture Mechanics*, **76** (2009), No. **8**, 2799–2809.

[117] de Morais, A.B., A.B. Pereira, M.F.S.F. de Moura, A.G. Magalhães. Mode III Interlaminar Fracture of Carbon/epoxy Laminates using the Edge Crack Torsion (ECT) test. *Composites Science and Technology*, **69** (2009), No. **5**, 670–676.

[118] de Morais, A.B., A.B. Pereira, M.F.S.F. de Moura. Mode III Interlaminar Fracture of Carbon/epoxy Laminates using the Six-Point Edge Crack Torsion (6ECT). *Composites Part A: Applied Science and Manufacturing*, **42** (2011), No. **11**, 1793–1799.

[119] de Morais, A.B., A.B. Pereira. Mode III Interlaminar Fracture of Carbon/epoxy Laminates using a Four-point Bending Plate Test. *Composites Part A: Applied Science and Manufacturing*, **40** (2009), No. **11**,1741–1746.

[120] Pereira, A.B., A.B. de Morais, M.F.S.F. de Moura. Design and Analysis of a New Six-point Edge Crack Torsion (6ECT) Specimen for Mode III Interlaminar Fracture Characterisation. *Composites Part A: Applied Science and Manufacturing*, **42** (2011), No. **2**, 131–139.

[121] Donaldson, S. L. Mode III Interlaminar Fracture Characterization of Composite Materials. *Composite Science and Technology,* **32** (1988), No. **2**, 225–249.

[122] Martin, R. H. Evaluation of the Split Cantilever Beam for Mode III Delamination Testing. *Composite materials: fatigue and fracture, ASTM STP 1110,* **3** (1991), No. **3**, 423–266.

[123] Robinson, P., D. Q. Song. The Development of an Improuved Mode III Delamination Test for Composites. *Composite Science and Technology*, **52** (1994), No. **3**, 217–233.

[124] Becht, G., J. W. Gillespie. Design and Analysis of the Crack Rail Shear Specimen for Mode III Interlaminar Fracture. *Composite Science and Technology*, **31** (1988), No. **4**, 143–157.

[125] Becht, G., J. W. Gillespie. Numerical and Experimental Evaluation of the Mode III Intrerlaminar Fracture Toughness of Composite Materials. *Polymer Composites*, **10** (1989), No. **5,** 34–51.

[126] Sharif, F., M. T. Kortschot, R. H. Martin. Mode III Delamination using a Split Cantilever Beam. In: Composite Materials: Fatigue and Fracture, ASTM STP, **5** (1995), No. **1**, 85–99.

[127] Rizov, V., Y. Shindo, K. Horiguchi, F. Narita. Mode III Interlaminar Fracture Behaviour of Glass Fibre Reinforced Polymer Woven Laminates at 293 K to 4 K. *Applied Composite Materials*, **13** (2006), No. **5**, 287–304.

[128] Sih, G. C., P. C. Paris, G. R. Irwin. On Cracks in Rectilinearly Anisotropic Bodies. *International Journal of Fracture Mechanics*, **1** (1965), No. **1**, 189–203.

[129] Zhao, D., Y. Wang. Mode III Fracture Behaviour of Laminated Composite with Edge Crack in Torsion. *Theoretical and Applied Fracture Mechanics,* **29** (1998), No. **3**, 109–123.

[130] Whitney, J. M. Experimental Characterization of Delamination Fracture. In: Interlaminar response of composite materials, (Ed. N. J. Pagano), Amsterdam: Elsevier (1989), 161–250.

[131] Johannesson, T., M. Blikstadt. Fractography and Fracture Criteria of the Delamination Process, In: Delamination and Debonding of Materials, ASSTM STP 876, Philadelphia (Ed. W. S. Johnson), (1985), 411–423.

[132] Hahn, H. T. A Mixed-mode Fracture Criterion for Composite Materials. *Composite Technology Review*, **5** (1983), No. **1**, 26–29.

[133] Richard, H. A. Safety Estimation for Construction Units with Cracks under Complex Loading, In: Structural Failure Product Liability and Technical Insurance, Proc. of 2-nd Int. Conf. July 1-3, Austria, Vienna, Geneva: Inderscience (Ed. Rossmanith H. P.), 1986, 423–437.

[134] Yan, X. Q., S. Y. Du, D. Wang. An Engineering Method of Determining the Delamination Fracture Toughness of Composite Laminates. *Engineering Fracture Mechanics*, **39** (1997), No. **4**, 623–627.

[135] Kaszmarek, K., M. R. Wisnm, M. I. Jones. Edge Delamination in Curved Glass-fibre/epoxy Beams Loaded in Bending. *Composites Science and Technology*, **58** (1998), No. **4**, 155–161.

[136] Kulkarni, N., H. Mahfuz, S. Jeelani, L. A. Carlsson. Fatigue Crack Growth and Life Prediction of Foam Core Sandwich Composites under Flexural Loading. *Composite Structures*, **59 (**2003), No. **4**, 499–505.

[137] Can, W, C. Hao-ran, L. Zhen-kun. Experimental Investigation of Interfacial Fracture Behaviour in Foam Core Sandwich Beams with Viscous-elastic Adhesive Interface. *Composite Structures*, **92** (2010), No. **5**, 1085–1091.

[138] Rinker, M., M. John, P. C. Zahlen, R. Schäuble. Face Sheet Debonding in CFRP/PMI Sandwich Structures under Quasi-static and Fatigue Loading Considering Residual Thermal Stress. *Engineering Fracture Mechanics*, **78** (2011), No. **17**, 2835–2847.

[139] Reyes, G., S. Rangaraj. Fracture Properties of High Performance Carbon Foam Sandwich Structures. *Composites Part A: Applied Science and Manufacturing*, **42** (2011), No. **1**, 1–7.

[140] Corigliano, A., E. Rizzi, E. Papa. Experimental Characterization and Numerical Simulations of a Syntactic-foam/glass-fibre Composite Sandwich. *Composites Science and Technology*, **60** (2000), No. **11**, 2169–2180.

[141] Rangaraj, S. Influence of Skin/core Debonding on Free Vibration Behaviour of Foam and Honeycomb Cored Sandwich Plates. *International Journal of Non-Linear Mechanics*, **45** (2010), No. **10**, 959–968.

[142] David, R., K. Veazie, R. Robinson, K. Shivakumar. Effects of the Marine Environment on the Interfacial Fracture Toughness of PVC Core Sandwich Composites. *Composites Part B: Engineering*, **35** (2004), No. **6–8**, 461–466.

[143] Quispitupa, A., C. Berggreen, L.A. Carlsson. On the Analysis of a Mixed Mode Bending Sandwich Specimen for Debond Fracture Characterization. *Engineering Fracture Mechanics*, **76** (2009), No. **4**, 594–613.

[144] Srinivasagupta, D., B. Joseph, P. Majumdar, H. Mahfuz. Effect of Processing Conditions and Material Properties on the Debond Fracture Toughness of Foam-core Sandwich Composites: Process Model Development. *Composites Part A: Applied Science and Manufacturing*, **34** (2003), No. **11**, 1085–1095.

[145] Ramantani, D. A., M.F.S.F. de Moura, R.D.S.G. Campilho, A.T. Marques. Fracture Characterization of Sandwich Structures Interfaces under Mode I Loading. *Composites Science and Technology*, **70** (2010), No. **9**, 1386–1394.

[146] Shi-Dong Pan, Lin-Zhi Wu, Yu-Guo Sun, Zheng-Gong Zhou. Fracture Test for Double Cantilever Beam of Honeycomb Sandwich Panels. *Materials Letters*, **62** (2008), No. **3**, 523–526.

[147] Cantwell, W. J., R. Scudamore, J. Ratcliffe, P. Davies. Interfacial Fracture in Sandwich Laminates. *Composites Science and Technology*, **59** (1999), No. **14**, 2079–2085.

[148] Goswami, S., W. Becker. The Effect of Face Sheet/core Delamination in Sandwich Structures under Transverse Loading. *Composite Structures*, **54** (2001), No. **3**, 515–521.

[149] Rizzi, E., E. Papa, A. Corigliano. Mechanical Behaviour of a Syntactic Foam: Experiment and Modelling. *International Journal of Solids and Structures*, **37** (2000), No. **5**, 5773–5794.

[150] Bazhant, Z. P., Y. Zhou, G. Zi, I. M. Daniel. Size Effect and Asymptotic Matching Analysys of Fracture of Closed-cell Polymeric Foam. *International Journal of Solids and Structures*, **40** (2003), No. **2**, 7197–7217.

[151] Ashby, M. F., L. J. Gibson, S. K. Maiti. Fracture Toughness of Brittle Cellular Solids. *Scr. Metall.*, **18** (1984), No. **5**, 213–217.

[152] Fowlkes, C. W. Fracture Toughness Tests of Rigid Polyurethane Foam. *International Journal of Fracture*, **10** (1974), No. **6**, 99–108.

[153] McIntyre, A., G. E. Anderton. Fracture Properties of a Rigid Polyurethane Foam over a Range of Densities. *Polymer*, **20** (1979), No. **5**, 247–253.

[154] Rizov, V. I. Non-linear Indentation Behaviour of Foam Core Sandwich Composite Materials-A 2D Approach. *Computational Materials Science*, **35** (2006), No. **2**, 107–115.

[155] Rizov, V. Failure Behaviour of Composite Sandwich Structures under Local Loading. *Archive of Applied Mechanics*, **79** (2009), No. **3**, 205–212.

[156] Rizov, V.I. Elastic-plastic Response of Structural Foams Subjected to Localized Static Loads. *Materials and Design*, **27** (2006), No. **10**, 947–954.

[157] Rizov, V., A. Shipsha, D. Zenkert. Indentation Study of Foam Core Sandwich Composite Panels. *Composite Structures*, **69** (2005), No. **1**, 95–102.

[158] Rizov, V., A. Mladensky. Influence of the Foam Core Material on the Indentation Behaviour of Sandwich Composite Panels. *Cellular Pollymres*, **26** (2007), No. **2**, 117–131.

[159] Rizov, V. Indentation of Foam-based Polymer Composite Sandwich Beams and Panels under Static Loading. *Journal of Materials Engineering and Performance*, **18** (2009), No. **4**, 351–360.

[160] Rizov, V. I., T. Harmia, A. Reinhardt, K. Friedrich. Fracture Toughness of Discontinuous Long Glass Fiber Reinforced Polypropylene: An Approach Based on a Numerical Prediction of Fiber Orientation in Injection Moulding. *Polymers and Polymer Composites*, **13** (2005), No. **2**, 121–130.

[161] Rizov, V., A. Mladensky. Non-linear Fracture Study of Glass Fibre Reinforced Polymer Composites using a Tapered Double Cantilever Beam. *Multidiscipline Modelling in Materials and Structures*, **5** (2009), No. **4**, 363–366.

[162] Rizov, V. Non-linear Fatigue Fracture Analysis of Composite Laminates. *Polymers and Polymer Composites*, **17** (2009), No. **6**, 371–377.

[163] Rizov, V., A. Mladensky. Fracture Toughness of Laminated Composites – a Non-linear Analysis. *Polymers and Polymer Composites*, (accepted for publication in 2011).

To be continued.